FOREX Publication
Open Access | Rapid and quality publishing

International Journal of
Electrical and Electronics Research (IJEER)
Research Article | Volume 13, Issue 2 | Pages 296-305| e-ISSN: 2347-470X

# A Lightweight CNN Architecture for Efficient Brain Tumor Detection in MRI Scans

**Yasser Nizamli[1,2*], Anton Filatov[1], Weaam Fadel[3], Yulia Shichkina[3], Kinda Mreish[4,5]**

[1]*Department of Software Engineering and Computer Applications, Saint Petersburg Electrotechnical University "LETI", Saint Petersburg, Russia*
[2]*Department of Computer Engineering and Automatic Control, Latakia University, Latakia, Syria*
[3]*Department of Computer Engineering, Saint Petersburg Electrotechnical University "LETI", Saint Petersburg, Russia*
[4]*Department of Computer Engineering, Aleppo University, Aleppo, Syria*
[5]*Department of Information Systems, Saint Petersburg Electrotechnical University "LETI", Saint Petersburg, Russia*

***Correspondence:** *yanizamli@stud.etu.ru*

**ABSTRACT-** The intricate morphology of brain tumors poses significant diagnostic challenges in MRI interpretation. While AI-driven systems offer potential for automation, balancing accuracy with computational efficiency remains critical for clinical adoption. This work introduces a lightweight convolutional neural network optimized for brain tumor detection and classification in MRI scans. The architecture's design emphasizes a systematic exploration of layer-ordering strategies, with experiments revealing that batch normalization in post-activation mode (Post-BN) outperforms Pre-BN in training stability and classification accuracy. Contrary to expectations, integrating shortcut connections for residual learning demonstrated negligible performance gains. Evaluated on the Figshare (multi-class) and Br35H (binary) datasets, the model achieves state-of-the-art accuracy while maintaining resource efficiency through minimized parameters and FLOPs. These findings highlight the importance of strategic layer ordering over architectural complexity in deep learning for medical imaging, offering a framework for efficient and reliable tumor detection that could generalize to other vision-based diagnostic tasks.

**Keywords:** Brain tumor detection, medical imaging, MRI images, Deep learning, Lightweight CNN, Batch normalization, Residual connections, Figshare dataset, Br35H dataset.

**ARTICLE INFORMATION**

**Author(s)**: Yasser Nizamli, Anton Filatov, Weaam Fadel, Yulia Shichkina and Kinda Mreish;
**Received**: 24/04/2025; **Accepted**: 02/06/2025; **Published**: 18/06/2025;
**E- ISSN**: 2347-470X;
**Paper Id**: IJEER 2404-09;
**Citation**: 10.37391/ijeer.130213
**Webpage-link:**
https://ijeer.forexjournal.co.in/archive/volume-13/ijeer-130213.html

**Publisher's Note:** FOREX Publication stays neutral with regard to jurisdictional claims in Published maps and institutional affiliations.

## 1. INTRODUCTION

### 1.1. Clinical context and diagnostic challenges

When the mechanisms that maintain cellular balance are disrupted, abnormal cell division occurs, leading to the formation of tumors. If this uncontrolled growth affects brain tissue, it results in a brain tumor. Brain tumors can be either benign, characterized by slow growth and well-defined borders, or malignant, which grow rapidly and have the potential to invade surrounding tissues. Based on their cellular origin, brain tumors are primarily classified into gliomas, meningiomas, or pituitary tumors. Gliomas, originating from glial cells, are typically aggressive and account for the majority of malignant brain tumors. In contrast, meningiomas and pituitary tumors are often benign, with the former arising from arachnoid cells and the latter from pituitary gland cells [1, 2, 3, 4]. Accurate and timely diagnosis of brain tumors is critical for determining the most appropriate treatment strategy based on the tumor's type and grade. Magnetic resonance imaging (MRI), when available, is the preferred diagnostic tool due to its ability to provide high-contrast images of the brain's soft tissues [4, 5, 6]. However, MRI diagnosis is often costly and time-consuming compared to other methods, which can delay treatment. Manual interpretation, relying on expertise and experience, is prone to human error, particularly in complex cases. Furthermore, this approach struggles to handle large datasets efficiently, especially as the workload increases [7, 8]. Automated systems leveraging machine learning and deep learning have addressed many of these challenges, with the scientific community developing numerous models to enhance the accuracy and efficiency of brain tumor detection [9, 10].

### 1.2. Critical review of automated approaches

Recent advances in deep learning have yielded multiple promising systems for detecting brain anomalies in medical imaging. *Table 1* provides an overview of the models presented in the published literature. Researchers in [3] introduced a CNN model designed to classify major brain tumors using MRI images. The network architecture comprises ten consecutive convolutional layers, with each pair followed by a pooling element. The features extracted from these layers are flattened and fed into a two-layer neural classifier, achieving an accuracy of 94.74%. However, the model struggled with meningioma classification, yielding an F1 score of only 89.68%, which suggests class-specific performance bias. In [4], a specialized

FOREX Publication
Open Access | Rapid and quality publishing
International Journal of Electrical and Electronics Research (IJEER)
Research Article | Volume 13, Issue 2 | Pages 296-305| e-ISSN: 2347-470X

CNN was proposed, consisting of three convolution-pooling blocks followed by a fully connected neural network. The model demonstrated accuracies of 99.31% and 93.1% for training and testing, respectively, surpassing traditional handcrafted feature extraction methods such as GLCM and GLDM. Notably, the significant performance gap between training and testing phases highlights potential overfitting to the training dataset. Similarly, a study in [5] employed a feature extractor with three convolution-pooling blocks and a four-layer fully connected neural network. This model achieved a training accuracy of 99.21%, while its testing accuracy reached 95.87%. Critically, class imbalance severely impacted minority-class accuracy, which ranged from 21.3% (with Adagrad) to 89.8% (with RMSprop). In [9], researchers developed a five-block convolution-pooling system for feature extraction from MRI images. The extracted features were then classified using either a two-layer neural network or an SVM algorithm, with the former achieving 95.42% accuracy and the latter slightly outperforming it at 96%. The inclusion of Anisotropic Diffusion Filter (ADF) and Adaptive Histogram Equalization (AHE) in preprocessing introduces computational overhead and deployment challenges. Another approach in [10] involved a model with three parallel convolutional networks, each containing five convolution-pooling blocks. The features from these networks were either combined and passed to a k-NN classifier or processed separately by three k-NN instances using majority voting. The first approach achieved an accuracy of 95.3%, while the second reached 95.6%. However, using k-NN as the final classifier reduces scalability, as the entire training dataset must be stored and processed during inference. Additionally, reliance on the first nearest neighbor (1-NN) rule increases sensitivity to noise and outliers.

Beyond custom-built systems, retraining standard models offers a practical alternative that circumvents the need to develop specialized architectures from scratch. Reference [11] introduces a lightweight approach for brain anomaly detection in MRI scans, combining the YOLOv5m framework with an Enhanced Spatial Attention (ESA) mechanism. This hybrid configuration demonstrates improved performance with 92% precision and 87.8% recall, surpassing the baseline YOLOv5m results. A related investigation by researchers in [12] employed the YOLOv8s architecture, which reached 94.2% precision and 90.8% recall. For both studies, the F1 score derived from the harmonic mean of precision and recall yields values of 89.86% for the YOLOv5m variant and 92.47% for the YOLOv8s implementation. However, given the critical role of brain tumor detection in clinical decision-making, where diagnostic accuracy directly affects treatment planning and patient survival, these YOLO models still require substantial performance improvements to meet the rigorous reliability standards expected in medical practice.

To reduce the computational burden of training deep networks, pre-trained benchmark networks are often utilized. In [13], the weights of the InceptionV3 and Xception models, previously trained on the ImageNet dataset, are frozen and employed as feature extractors for MRI images. The extracted features are then fed into an ensemble classifier comprising three algorithms: k-NN, SVM, and RF. The model based on InceptionV3 features achieves an accuracy of 94.34%, while the Xception-based model reaches a slightly lower accuracy of 93.79%. In [14], researchers proposed a brain tumor detection system using the pre-trained VGG16 model. Deep features are extracted from denoised MRI images and classified using a neural network, achieving an accuracy of 96.01%. This high performance was achieved exclusively with geometric augmentation techniques, but accuracy dropped to 92.33% for the original unmodified dataset. Similarly, in [15], the DenseNet169 model was integrated into a brain tumor recognition system. Numerical features extracted from the model are classified using a majority voting approach among RF, SVM, and XGBoost classifiers, resulting in a reported accuracy of 95.10%. While transfer learning models reduce training costs, their extreme depth (InceptionV3 with 94 convolutional layers and DenseNet169 with 87) introduces impractical computational demands during inference. This trade-off becomes critical in clinical settings, where latency and hardware limitations prioritize lightweight, specialized architectures over general-purpose pre-trained networks.

It can be observed that the developed models mainly suffer from insufficient accuracy, high complexity, and inadequately addressed overfitting, as evidenced by the observed gap between training and testing performance. Employing pre-trained models with frozen weights can mitigate overfitting caused by training networks with millions of parameters. However, the high dimensionality of extracted features can lead traditional classifiers to fail in generalizing to test data.

**Table 1. Summary of recent related literature**

| Ref. | Dataset used | Data classes | Data splitting | Augmentation | Feature extraction | Classification | Performance |
|---|---|---|---|---|---|---|---|
| [3] | Figshare brain MRI dataset | Meningiomas, gliomas, and pituitary tumors | Five-fold CV | Not used | Ten-layer CNN | Two-layer neural classifier | ACC: 94.74% |
| [4] | Figshare brain MRI dataset | Meningiomas, gliomas, and pituitary tumors | Hold-out (70:30) | Color-space and geometric transformations | Three-block CNN | Neural classifier | ACC: 93.1% |

FOREX Publication
Open Access | Rapid and quality publishing
International Journal of Electrical and Electronics Research (IJEER)
Research Article | Volume 13, Issue 2 | Pages 296-305| e-ISSN: 2347-470X

| | | | | | | | |
|---|---|---|---|---|---|---|---|
| [5] | Figshare brain MRI dataset | Meningiomas, gliomas, and pituitary tumors | Hold-out (70:30) | Not stated | Three-block CNN | Four-layer neural classifier | ACC: 95.87% |
| [9] | Figshare brain MRI dataset | Meningiomas, gliomas, and pituitary tumors | Hold-out (80:20) | Geometric transformations | Five-block CNN | Two-layer neural classifier | ACC: 95.42% |
| | | | | | | SVM | ACC: 96% |
| [10] | Figshare brain MRI dataset | Meningiomas, gliomas, and pituitary tumors | Train-test-validation (60:20:20) | GAN Augmentation | Three parallel CNNs | KNN | ACC: 95.3% |
| | | | | | | Ensemble learning | ACC: 95.6% |
| [11] | Figshare brain MRI dataset | Meningiomas, gliomas, and pituitary tumors | Five-fold CV | Copy-paste augmentation, color-space and geometric transformations | Modified YOLOv5m | Neural classifier | F1: 89.86% |
| [12] | Figshare brain MRI dataset | Meningiomas, gliomas, and pituitary tumors | Train-test-validation | Color-space and geometric transformations | YOLOv8s | Neural classifier | F1: 92.47% |
| [13] | Figshare brain MRI dataset | Meningiomas, gliomas, and pituitary tumors | Hold-out (80:20) | Not stated | Inception-v3 | Ensemble learning | ACC: 94.34% |
| | | | | | Xception | | ACC: 93.79% |
| [14] | Figshare brain MRI dataset | Meningiomas, gliomas, and pituitary tumors | Ten-fold CV | Color-space and geometric transformations | VGG16 | Neural classifier | ACC: 96.01% |
| [15] | Figshare brain MRI dataset | Meningiomas, gliomas, and pituitary tumors | Hold-out (80:20) | Geometric transformations | DenseNet169 | Ensemble learning | ACC: 95.10% |

### 1.3. Research objectives and contributions

In this study, we aim to address the challenges discussed above, with our main contributions outlined as follows:

- Proposing a specialized deep learning model for brain tumor detection in MRI images that balances low complexity (in terms of parameter count and FLOPs) with high performance (in terms of classification accuracy).
- Investigating the impact of batch normalization in both pre-activation and post-activation modes to determine the optimal approach for the proposed network.
- Exploring the effectiveness of incorporating residual connections into few-layer convolutional neural network architectures.
- Evaluating modified instances of the proposed system on two independent datasets using a variety of evaluation metrics.

### 1.4. Paper organization

The remainder of the paper is structured as follows: The Materials and Methods section outlines the datasets employed, along with the components and operational details of the proposed model. The Results and Discussion section presents the experimental outcomes and their analysis. The Limitations and Future Work section discusses the current shortcomings of our approach and potential directions for improvement. Finally, the Conclusion section summarizes the core contributions and insights of the research.

## 2. MATERIALS AND METHODS

### 2.1. Data sets and preprocessing

This study aims to enhance the efficiency of brain tumor classification in MRI images. To ensure the reliability of the results, the proposed model requires a high-quality dataset for training and evaluation. The primary dataset used in this work is the Figshare brain tumor MRI dataset, which was gathered from 223 patients by a team of experts and specialists across multiple hospitals in China and made publicly accessible for research purposes [16]. The dataset comprises 3064 samples categorized into three tumor types: 708 meningiomas, 1426 gliomas, and 930 pituitary tumors. The *figshare* dataset is one of the few MRI data sources that have been systematically organized and processed, enhancing the credibility of models validated using it.

Testing the proposed model on an independent dataset provides robust validation of its effectiveness. The second MRI dataset employed in this work is the Br35H: Brain Tumor Detection 2020 dataset, publicly available on Kaggle and commonly used in research [17, 18, 19]. This dataset contains 3000 samples, evenly split into 1500 normal images and 1500 brain tumor images, offering a well-balanced platform for evaluation.

The preprocessing pipeline involves only resizing all images to 224 × 224 pixels before inputting them into the network. This minimal approach enhances inference speed and system efficiency, as complex preprocessing steps applied during

FOREX Publication
Open Access | Rapid and quality publishing
International Journal of Electrical and Electronics Research (IJEER)
Research Article | Volume 13, Issue 2 | Pages 296-305| e-ISSN: 2347-470X

training would need to be replicated during deployment to maintain consistency and reproducibility [20]. Additionally, unlike the perfectly balanced Br35H dataset, the Figshare dataset exhibits a natural, non-extreme imbalance that reflects real-world clinical prevalence. Introducing synthetic samples through augmentation risks generating unrealistic artifacts in MRI scans, which could compromise model reliability. Instead of relying on data balancing or augmentation, this work prioritizes a robust architectural design that learns generalizable features rather than overfitting to the majority class. *Figure 1* displays representative samples from the datasets utilized in this work.

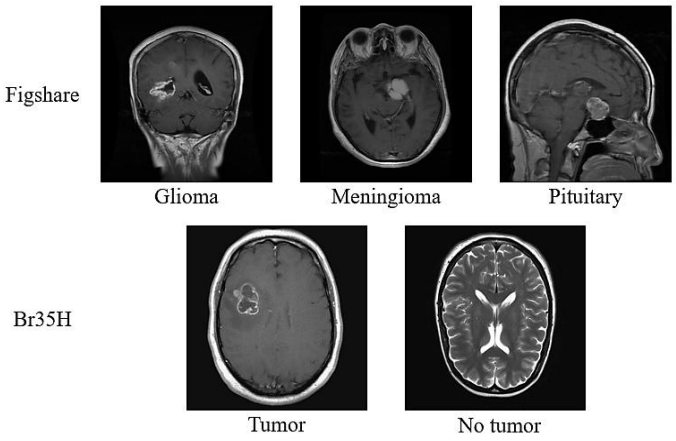


**Figure 1.** Samples from the datasets employed in the study

## 2.2. Baseline CNN architecture

*Figure 2* illustrates three variations of the proposed CNN model designed for detecting brain abnormalities in MRI images, each featuring slightly distinct architectures. The foundational model (*figure 2a*) comprises five sequential convolutional blocks. Within each block, a Conv2D layer is followed by a batch normalization (BN) element and a ReLU activation function. The convolutional layers are responsible for extracting spatial features, such as edges and textures, from the input images. The BN layer standardizes these features to enhance and accelerate the learning process, while the ReLU activation introduces nonlinearity, enabling the network to model complex patterns. Following the first and fifth convolutional blocks, a Pooling2D layer is included to down sample the input volume, effectively reducing computational complexity. After the final pooling layer, a flattening layer transforms the output volume into a one-dimensional array, which is then fed into a fully connected network. The neural classifier is structured into three layers: two dense layers, each preceded by a dropout element and followed by a ReLU function, and a final dense output layer with a softmax activation. The dropout layer functions as a regularization technique, reducing the risk of overfitting by randomly deactivating subsets of neurons during the training process. The softmax activation function transforms the network's output into a probability distribution, assigning likelihood values to each class. Consequently, the network processes a brain MRI image as its input and generates an output representing the probability of the image belonging to each class, as defined by the training dataset.

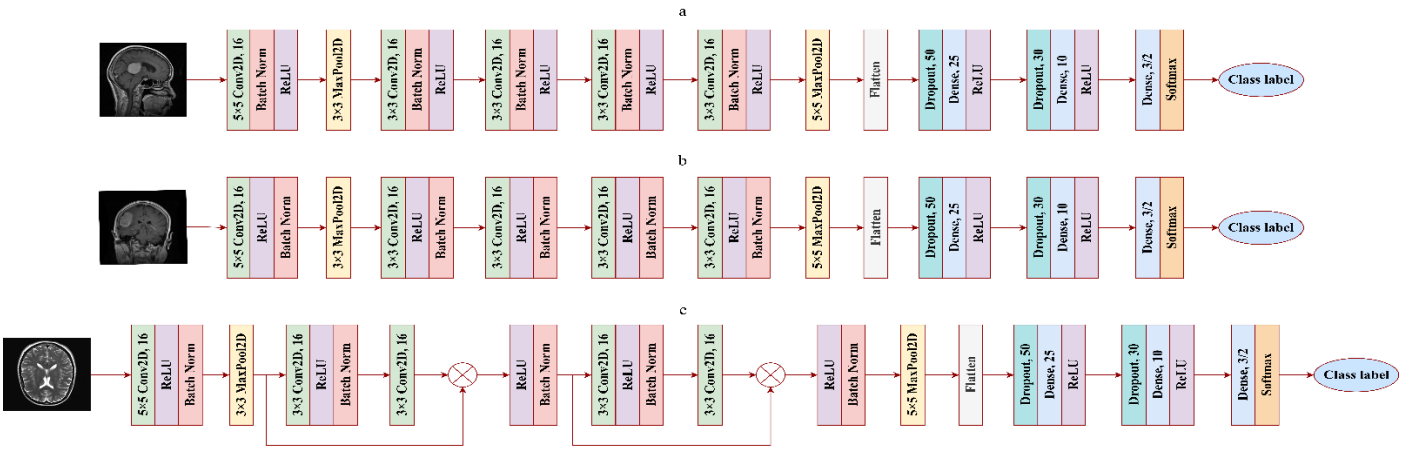


**Figure 2.** Proposed CNN instances: (a) Plain CNN with batch normalization in pre-activation mode (Pre-BN CNN), (b) Plain CNN with batch normalization in post-activation mode (post-BN CNN), (c) Residual CNN with batch normalization in post-activation mode (post-BN Res CNN)

## 2.3. Architectural variants: BN placement and residual connections

The initial network employs batch normalization in pre-activation mode, where normalization is applied to the linear output of the convolution prior to the ReLU activation. This configuration, referred to as Pre-BN CNN, is a widely adopted approach in many models, particularly those designed for natural images [21, 22]. However, medical images such as MRIs exhibit distinct intensity distributions that may not align well with this architecture. Specifically, zero mean/unit variance normalization can result in many feature values becoming negative, which are subsequently eliminated by the ReLU activation. This increases sparsity and risks the loss of potentially discriminative features critical for MRI image analysis. Despite the widespread adoption of pre-activation normalization in brain MRI anomaly detection models [9, 15, 23, 24], the impact of normalization layer placement on medical imaging systems remains understudied. Existing work often treats pre-activation as a default practice without rigorously evaluating how this design choice affects

FOREX Publication
Open Access | Rapid and quality publishing
International Journal of Electrical and Electronics Research (IJEER)
Research Article | Volume 13, Issue 2 | Pages 296-305| e-ISSN: 2347-470X

training dynamics or model performance. To address this issue, the second version of the system, depicted in *figure 2b*, proposes a modification to the convolutional block. In this revised architecture, normalization is applied to the activated features, meaning the Conv2D layer is followed by the ReLU activation function and then the BN layer. This configuration, termed plain CNN with BN in post-activation mode (post-BN CNN), will be evaluated to assess its influence on performance and training dynamics.

A potential strategy for boosting the performance of specialized CNN systems involves the utilization of shortcut connections, also referred to as skip connections. These connections create pathways that bypass one or more network blocks, linking the output of one layer to a layer further ahead in the architecture. Skip connections enable more efficient gradient flow during backpropagation and allow the network to reuse features from earlier layers, which can enhance learning capabilities. In this study, we explore the effectiveness of employing shortcut connections to design a residual network for brain tumor detection, as illustrated in *figure 2c*. The post-BN CNN is adjusted by introducing two skip connections: the first connects the output of the first Pooling2D layer (which acts as the input to the second convolutional block) to the output of the third Conv2D layer, while the second links the output of the third convolutional block (the input to the fourth Conv2D layer) to the output of the fifth Conv2D layer. This adapted architecture is referred to as post-BN Res CNN, combining residual learning principles with the post-activation batch normalization approach.

## 2.4. Detailed architecture specifications

The microarchitecture of the proposed approach is detailed in *table 2*. A consistent and modest number of filters is applied across all convolutional layers. This design choice reduces the parameter count and may facilitate more efficient generalization compared to hierarchical approaches, particularly when working with limited dataset sizes. The initial convolutional layer utilizes 5×5 filters to capture coarse spatial context, which is beneficial for learning low-level features in early layers. Subsequent layers switch to 3×3 filters to achieve finer-grained representations and reduce computational complexity. Pooling layers employ relatively large windows to effectively downsample spatial dimensions, with aggressive downsampling in Pool_2 ensuring the selection of the most informative high-level features after a series of consecutive convolutions. The largest number of parameters lies between the flattening layer and the first fully connected layer, making it logical to insert a dropout element with a high ratio to mitigate overfitting. It is important to note that the structure outlined in *table 2* primarily describes the Pre-BN CNN model. The Post-BN CNN and Post-BN Res CNN models differ only in the placement of normalization layers and the inclusion of skip connections, without altering the microarchitecture. Despite having the same number of parameters across all versions, the residual network incurs a slight increase in computational cost due to the additional element-wise addition operations.

**Table 2. Proposed structure details**

| Layer | Type | Kernal size | #Filters | Stride | Padding | Output shape | #Param |
|---|---|---|---|---|---|---|---|
| Input_1 | Input layer | – | – | – | – | 224×224×3 | 0 |
| Conv_1 | Conv2D | 5×5 | 16 | 1 | same | 224×224×16 | 1216 |
| BN_1 | Batch norm | – | – | – | – | 224×224×16 | 64 |
| Act_1 | ReLU | – | – | – | – | 224×224×16 | 0 |
| Pool_1 | MaxPool2D | 3×3 | – | 3 | valid | 74×74×16 | 0 |
| Conv_2 | Conv2D | 3×3 | 16 | 1 | same | 74×74×16 | 2320 |
| BN_2 | Batch norm | – | – | – | – | 74×74×16 | 64 |
| Act_2 | ReLU | – | – | – | – | 74×74×16 | 0 |
| Conv_3 | Conv2D | 3×3 | 16 | 1 | same | 74×74×16 | 2320 |
| BN_3 | Batch norm | – | – | – | – | 74×74×16 | 64 |
| Act_3 | ReLU | – | – | – | – | 74×74×16 | 0 |
| Conv_4 | Conv2D | 3×3 | 16 | 1 | same | 74×74×16 | 2320 |
| BN_4 | Batch norm | – | – | – | – | 74×74×16 | 64 |
| Act_4 | ReLU | – | – | – | – | 74×74×16 | 0 |
| Conv_5 | Conv2D | 3×3 | 16 |  | same | 74×74×16 | 2320 |
| BN_5 | Batch norm | – | – | – | – | 74×74×16 | 64 |
| Act_5 | ReLU | – | – | – | – | 74×74×16 | 0 |
| Pool_2 | MaxPool2D | 5×5 | – | 5 | valid | 14×14×16 | 0 |
| Flatten_1 | Flatten | – | – | – | – | 3136 | 0 |
| Drop_1 | Dropout 50% | – | – | – | – | 3136 | 0 |
| FC_1 | Dense 25 | – | – | – | – | 25 | 78425 |
| Drop_2 | Dropout 30% | – | – | – | – | 25 | 0 |
| FC_2 | Dense 10 | – | – | – | – | 10 | 260 |
| FC_3 | Dense 3 | – | – | – | – | 3 | 33 |
| Act_6 | SoftMax | – | – | – | – | 3 | 0 |

FOREX Publication
Open Access | Rapid and quality publishing
International Journal of Electrical and Electronics Research (IJEER)
Research Article | Volume 13, Issue 2 | Pages 296-305| e-ISSN: 2347-470X

### 2.5. Hyperparameter configuration and training protocol

*Table 3* summarizes the hyperparameters adopted for all experiments. The Adam optimizer is selected to update the network weights based on the gradients of the loss function. To ensure consistency in the model structure, the output is converted to one-hot encoding, and a softmax activation is applied in the final layer for both binary and multi-class classification tasks, rather than using a single output neuron with a sigmoid function for binary brain tumor detection. This approach allows the use of the categorical cross-entropy loss function to quantify the difference between the predicted and actual probability distributions. A relatively small batch size is employed, enabling more frequent weight updates, which can enhance learning efficiency, particularly on smaller training datasets. Given that the primary activation function is ReLU, the He-normal initialization method is used to set the initial weights in the network.

While the computational complexity is roughly constant across all presented CNN models, performance and training dynamics are likely to exhibit notable variations. The following section details experimental results for both primary (multi-class brain tumor classification) and secondary (binary tumor detection) tasks.

**Table 3. Hyperparameter settings for model training**

| Hyperparameter | Adjustment |
|---|---|
| Optimizer | Adaptive moment estimation (Adam) |
| Loss function | Categorical cross entropy |
| Learning rate | 0.001 |
| Epochs | 200 |
| Initializer | He-Normal |
| Batch size | 8 |

## 3. EXPERIMENTS, RESULTS AND DISCUSSION

### 3.1. Experimental setup

All experiments were conducted in Google Colab, connected to a local notebook server running on a dedicated Anaconda environment. The hardware configuration features an NVIDIA GeForce RTX 4070 GPU with 8 GB VRAM, paired with a 12$^{th}$ Gen Intel Core i7-12650H processor and 16 GB system memory. For constructing convolutional networks, the TensorFlow machine learning framework and Keras deep learning API were utilized, both powered by CUDA 12.8 and cuDNN 8 for NVIDIA GPU acceleration. Three variants of the proposed model were trained and evaluated on two distinct datasets using two complementary validation strategies: holdout (80:20 split), where 80% of the data is allocated for training to optimize feature learning, and the remaining 20% is reserved for performance evaluation, and 5-fold cross-validation, a rigorous technique that partitions the dataset into five equal subsets, iteratively training the model on four folds and validating on the fifth to ensure statistical reliability and mitigate overfitting. This experimental design generated twelve distinct test cases, with their outcomes analyzed and presented in the following discussion.

### 3.2. Multi-class classification results

For the multi-classification of brain tumor types (Figshare dataset), the learning curves and classification report are presented in Figure 3 and Table 4, respectively. The accuracy versus epoch curve for the Pre-BN CNN exhibits pronounced oscillations and sudden jumps, reaching a final accuracy of only 94.12%. In contrast, modifying the architecture by placing BN after ReLU in the Post-BN CNN, then introducing skip connections in the Post-BN Res CNN, resulted in significantly smoother and more stable learning curves, with notable performance improvements. The accuracies rose to 98.04% and 98.86%, respectively. The confusion matrices in Figure 4 indicate that 36 samples were misclassified when normalization preceded activation, while this error reduced to only 12 samples for the Post-BN CNN and further declined to 7 samples with the residual network. These findings demonstrate the effectiveness of the Post-BN approach within the proposed specialized architecture, which enhanced overall performance, improved training dynamics, and stabilized weight updates through better feature representation and scale-consistent activations. Furthermore, the residual connections provided a very slight improvement in accuracy, attributable to enhanced gradient flow and feature reuse.

While data is shifted when selecting the training and testing sets in the common holdout approach for model evaluation, using a 5-fold cross-validation can provide a more robust estimate of performance without biasing toward a subset of the data. The bar charts in *figure 5* show the performance at each fold. The average accuracy across the test folds for the Pre-BN model was only 92±3.16%, while it achieved 96.80±0.59% for Post-BN CNN, and 96.80±0.52% for Post-BN Res CNN.

The paired t-test analysis of the 5-fold cross-validation accuracies across the three models reveals statistically significant differences between the Pre-BN CNN and Post-BN CNN (t=3.1151, p=0.0357) as well as between the Pre-BN CNN and Post-BN Res CNN (t=2.9308, p=0.0428), demonstrating that the order of normalization layers has a measurable impact on model performance. In contrast, the comparison between Post-BN CNN and Post-BN Res CNN yielded no statistical difference (t=0.0000, p=1.0000), indicating that adding a residual shortcut connection within this specific network architecture provides negligible practical improvement.

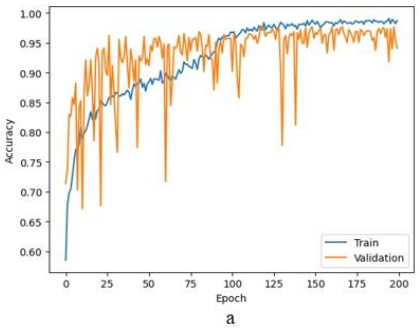

a

FOREX Publication
Open Access | Rapid and quality publishing
International Journal of Electrical and Electronics Research (IJEER)
Research Article | Volume 13, Issue 2 | Pages 296-305| e-ISSN: 2347-470X

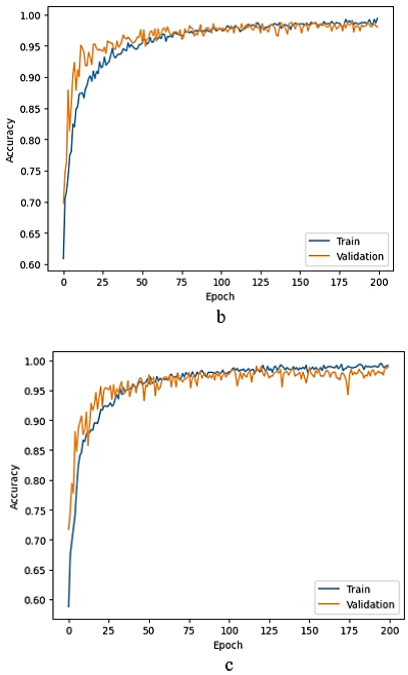


**Figure 3.** Learning curves for multi-class brain tumor classification (Figshare dataset): (a) Pre-BN CNN, (b) Post-BN CNN, (c) Post-BN Res CNN

**Table 4. Classification report for multi-class brain tumor classification (Figshare dataset)**

| Model | Category | Precision | Sensitivity | F1-score | Mean-F1 | ACC |
|---|---|---|---|---|---|---|
| Pre-BN CNN | Glioma | 99.60 | 89.21 | 94.12 | 93.76 | 94.12 |
| | Meningioma | 83.33 | 97.12 | 89.70 | | |
| | Pituitary | 96.02 | 98.97 | 97.47 | | |
| Post-BN CNN | Glioma | 98.20 | 98.20 | 98.20 | 97.79 | 98.04 |
| | Meningioma | 95.68 | 95.68 | 95.68 | | |
| | Pituitary | 99.49 | 99.49 | 99.49 | | |
| Post-BN Res CNN | Glioma | 99.64 | 98.56 | 99.10 | 98.70 | 98.86 |
| | Meningioma | 95.83 | 99.28 | 97.53 | | |
| | Pituitary | 100 | 98.97 | 99.48 | | |

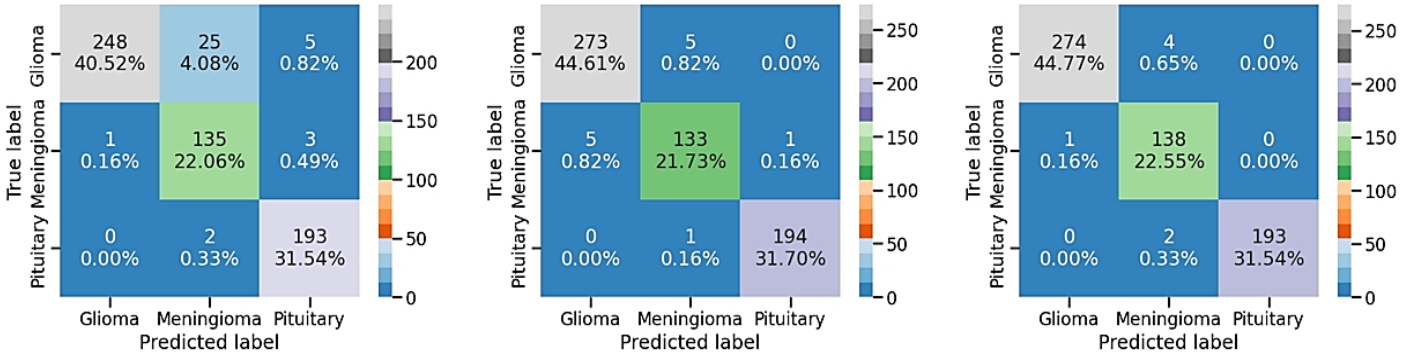


**Figure 4.** Confusion matrices for multi-class brain tumor classification (Figshare dataset): (a) Pre-BN CNN, (b) Post-BN CNN, (c) Post-BN Res CNN

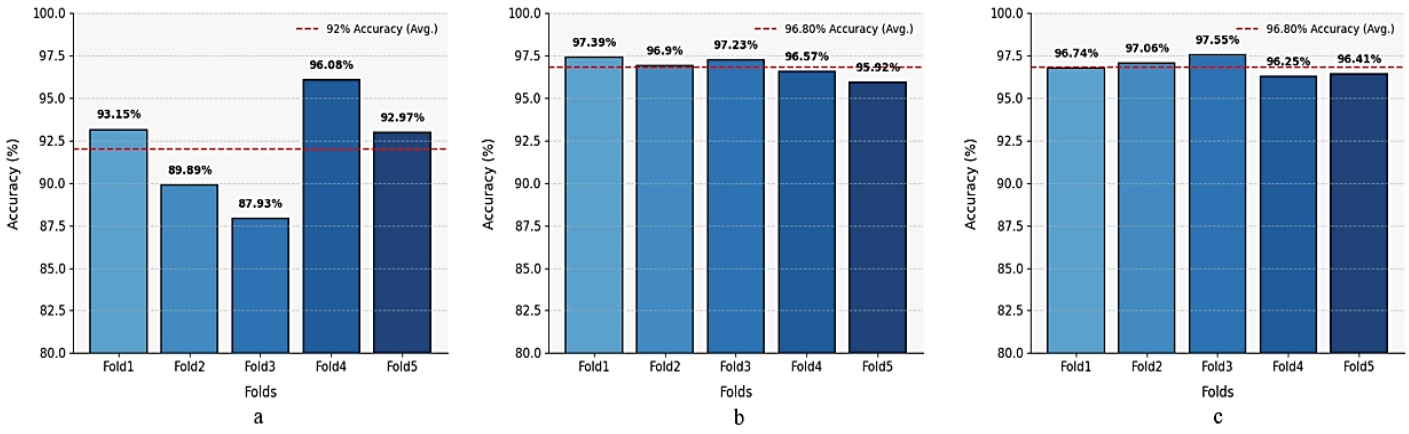


**Figure 5.** Performance by fold for multi-class brain tumor classification (Figshare dataset): (a) Pre-BN CNN, (b) Post-BN CNN, (c) Post-BN Res CNN

FOREX Publication
Open Access | Rapid and quality publishing
International Journal of Electrical and Electronics Research (IJEER)
Research Article | Volume 13, Issue 2 | Pages 296-305| e-ISSN: 2347-470X

### 3.3. Binary classification results

In the binary classification of brain MRIs (Br35H dataset), the learning curves remain stable across all cases, as illustrated in *figure 6*. *Table 5* presents classification results showing 97.83% accuracy for the Pre-BN CNN model compared to 99.17% for Post-BN variants. From the confusion matrices in *figure 7*, it is evident that 13 test samples were misclassified when normalization was applied immediately after convolution, whereas the error dropped to only 5 samples when batch normalization scaled the activation outputs. The 5-fold cross-validation results, presented in the bar charts of *figure 8*, demonstrate a tight convergence in performance among the evaluated models. Average accuracies across all test folds were 97.90±0.86% for Pre-BN CNN, 98.10±0.99% for Post-BN CNN, and 98.13±0.98% for Post-BN Res CNN. While minor numerical differences exist between models, comprehensive paired t-test analysis across all model combinations (Pre-BN vs. Post-BN, Pre-BN vs. Post-BN Res, and Post-BN vs. Post-BN Res) showed no significant differences (all p-values > 0.05), demonstrating that these minimal variations do not represent statistically meaningful enhancements. The strong performance of all models can likely be attributed to the relatively simpler nature of tumor detection compared to multi-class classification tasks. Additionally, the Br35H dataset is balanced, with an equal number of samples per class, and all images are in a single plane (axial), unlike the Figshare dataset, which includes axial, sagittal, and coronal views.

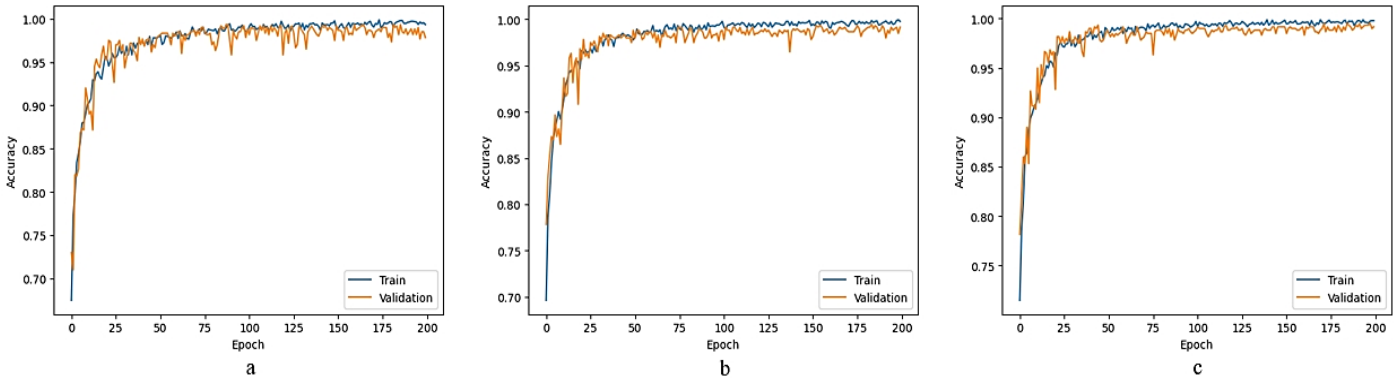


**Figure 6.** Learning curves for brain tumor detection (Br35H dataset): (a) Pre-BN CNN, (b) post-BN CNN, (c) post-BN Res CNN

**Table 5. Classification report for brain tumor detection (Br35H dataset)**

| Model | Category | Precision | Sensitivity | F1-score | Mean-F1 | ACC |
|---|---|---|---|---|---|---|
| Pre-BN CNN | No tumor | 98.96 | 96.61 | 97.77 | 97.83 | 94.12 |
| | Tumor | 96.79 | 99.02 | 97.89 | | |
| Post-BN CNN | No tumor | 99.66 | 98.20 | 99.15 | 99.17 | 99.17 |
| | Tumor | 98.70 | 99.67 | 99.18 | | |
| Post-BN Res CNN | No tumor | 99.66 | 98.56 | 99.15 | 99.17 | 99.17 |
| | Tumor | 98.70 | 99.67 | 99.18 | | |

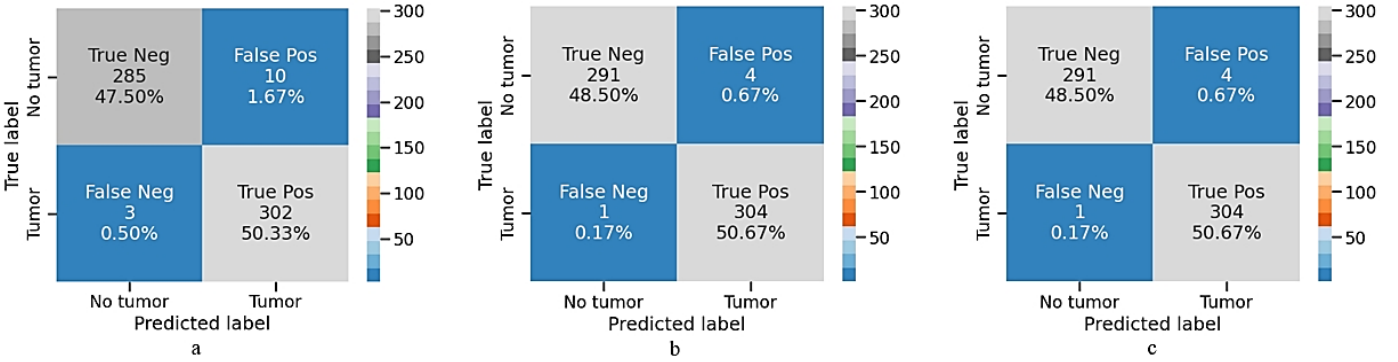


**Figure 7.** Confusion matrices for brain tumor detection (Br35H dataset): (a) Pre-BN CNN, (b) Post-BN CNN, (c) Post-BN Res CNN

FOREX Publication
Open Access | Rapid and quality publishing
International Journal of Electrical and Electronics Research (IJEER)
Research Article | Volume 13, Issue 2 | Pages 296-305| e-ISSN: 2347-470X

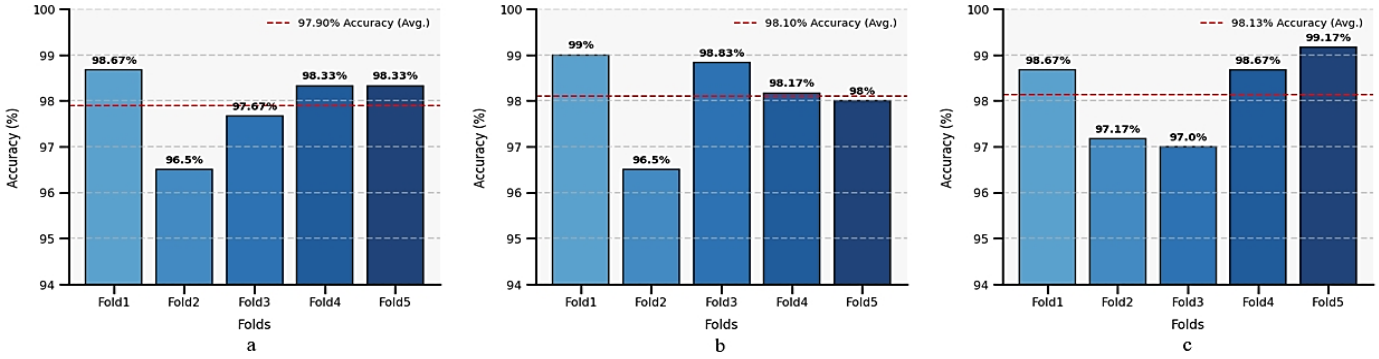


**Figure 8.** Performance by fold for brain tumor detection (Br35H dataset): (a) Pre-BN CNN, (b) Post-BN CNN, (c) Post-BN Res CNN

### 3.4. Computational complexity analysis

Regarding complexity analysis, parameter count and FLOPs provide clear insight into a model's computational efficiency. They offer more reliable evaluation of model complexity than training time since they quantify fixed architectural properties unaffected by hardware. Training time, however, varies substantially with computational resources. For example, using high-performance GPUs significantly reduces training duration, undermining its consistency for comparisons. In contrast, parameter counts and FLOP values remain stable across all computing platforms. As hardware-invariant measures, parameter count reflects total learned weights and biases, while FLOPs quantify floating-point operations per forward pass. These metrics reflect model size, inference speed, and deployment constraints. *Table 6* displays the parameter and FLOP counts for our network along with other models demonstrating these characteristics. The proposed model contains 89374 parameters across all instances, fewer than those in a single convolutional layer of many deep brain tumor detection models. Neither batch normalization placement nor skip connections influence the total parameter count. The FLOP count measures 0.2258 GFLOPs for both Pre-BN CNN and Post-BN CNN, with Post-BN Res CNN requiring slightly more at 0.2260 GFLOPs. When compared to the modified YOLOv5m model in [11], noted as lightweight with approximately 22 million parameters and 106 GFLOPs, our model demonstrates substantially lower complexity and superior computational efficiency, making it deployable on resource-constrained edge devices.

**Table 6. Computational complexity analysis: Parameter counts and floating-point operations**

| Ref. | Approach | FLOPs (GFLOPs) | Parameter count (M) |
|---|---|---|---|
| [3] | Custom CNN | – | 3.3 |
| [5] | Custom CNN | – | 13.1037 |
| [9] | Custom CNN | – | 0.9534 |
| [11] | YOLOv5m | 102.5 | 21.2 |
| [11] | Modified YOLOv5m | 106.3 | 22.1 |
| Proposed model | Pre-BN CNN | 0.2258 | 0.0894 |
| Proposed model | Post-BN CNN | 0.2258 | 0.0894 |
| Proposed model | Post-BN Res CNN | 0.2260 | 0.0894 |

### 3.5. Synthesis of key findings

The preceding analysis shows that proper arrangement of layers in the proposed network, particularly the batch normalization component and ReLU activation function, meaningfully influences overall performance and training behavior, especially for multi-class brain tumor classification. That said, including skip connections produced minimal improvement, likely because the network's modest size already allows effective gradient propagation. In addition to accuracy considerations, the model's internal architecture, comprising specific layer types along with carefully chosen filter numbers and dimensions, contributes to its computational efficiency.

## 4. LIMITATIONS AND FUTURE WORK

Despite the model's high performance and low computational complexity, its evaluation utilized datasets with limited tumor diversity. The Figshare dataset encompasses only meningiomas, gliomas, and pituitary tumors, while Br35H supports simple binary tumor/non-tumor classification. This restricted scope excludes clinically critical brain abnormalities such as medulloblastomas, schwannomas, and metastases, narrowing the model's diagnostic applicability. Furthermore, validation relied exclusively on computational metrics without practical clinical assessment comparing predictions against radiologist interpretations or measuring real-world workflow impact. To address these constraints, future efforts will expand tumor class coverage by acquiring datasets encompassing additional tumor types through hospital partnerships and parsing verified medical imaging repositories. Concurrently, thorough clinical investigations will be initiated through pilot deployments to evaluate the model's effectiveness in reducing diagnostic latency and improving early detection rates in real clinical settings.

## 5. CONCLUSIONS

This research introduces a lightweight, specialized convolutional neural network for detecting and classifying brain tumors in MRI scans. The architectural placement of batch normalization (BN) and rectified linear unit (ReLU) components proves crucial for performance, with the Post-BN CNN achieving better results than the Pre-BN CNN. Interestingly, incorporating shortcut connections to create a residual network architecture showed minimal performance

International Journal of Electrical and Electronics Research (IJEER)
Research Article | Volume 13, Issue 2 | Pages 296-305| e-ISSN: 2347-470X

impact. Comprehensive evaluation on both the Figshare dataset (multi-class tumor detection) and Br35H dataset (binary classification) demonstrates the model's strong performance across accuracy metrics while maintaining exceptional computational efficiency through optimized parameter counts and FLOPs. These findings underscore the significance of optimal layer ordering in deep models, which can enhance the automation of brain tumor detection in MRI scans and may extend to other computer vision applications.

**Author Contributions:** Yasser Nizamli: Conceptualization, Data curation, Formal analysis, Investigation, Methodology, Resources, Software, Validation, Visualization, Writing – original draft, Writing – review and editing. Anton Filatov: Conceptualization, Resources, Investigation, Validation, Supervision. Weaam Fadel: Conceptualization, Data curation, Formal analysis, Investigation, Methodology, Resources, Software, Validation, Visualization, Writing – original draft, Writing – review and editing. Yulia Shichkina: Conceptualization, Resources, Investigation, Validation, Supervision. Kinda Mreish: Conceptualization, Data curation, Formal analysis, Investigation, Methodology, Resources, Software, Validation, Visualization, Writing – original draft, Writing – review and editing.

**Funding Source:** This research has been supported by the Ministry of Science and Higher Education of the Russian Federation (assignment No. FSEE-2025-0015).

# REFERENCES

[1] Barkade, G.; Bhosale, P.; Shirsath, S. Overview of brain cancer, its symptoms, diagnosis and treatment. IP International Journal of Comprehensive and Advanced Pharmacology 2023, Volume 8, Issue 3, pp. 159–164.
[2] Alahmed, H.; Al-Suhail, G. Exploring transfer learning techniques for brain tumor diagnosis in MRI data. 2024 1st International Conference on Emerging Technologies for Dependable Internet of Things (ICETI), Sana'a, Yemen, 2024, pp. 1–8.
[3] Ayadi, W.; Elhamzi, W.; Charfi, I.; Atri, M. Deep CNN for brain tumor classification. Neural Processing Letters 2021, Volume 53, pp. 671–700.
[4] Sowrirajan, S. R.; Balasubramanian, S. Brain tumor classification using machine learning and deep learning algorithms. International Journal of Electrical and Electronics Research 2022, Volume 10, pp. 999–1004.
[5] Jaspin, K.; Selvan, S. Multiclass convolutional neural network-based classification for the diagnosis of brain MRI images. Biomedical Signal Processing and Control 2023, Volume 83.
[6] Perkins, A.; Liu, G. Primary Brain Tumors in Adults: Diagnosis and Treatment. Am Fam Physician 2016, Volume 93, Issue 3, pp. 211–217.
[7] Nizamli, Y.; Fadel, W.; Filatov, A.; Shichkina, Y. A new hybrid model for brain tumor recognition in MRI images based on hand-crafted features and deep learning. 2025 27th International Conference on Digital Signal Processing and its Applications (DSPA), Moscow, Russian Federation, 2025, pp. 1–4.
[8] Abda, O.; Naimi, H. Enhanced brain tumor MRI classification using stationary wavelet transform, ResNet50V2, and LSTM networks. ITEGAM-JETIA 2025, Volume 11, Issue 51, pp. 127–133.
[9] Biswas, A.; Islam, M. S. A hybrid deep CNN-SVM approach for brain tumor classification. Journal of Information Systems Engineering and Business Intelligence 2023, Volume 9, pp. 1–15.
[10] Deepak, S.; Ameer, P. M. Brain tumor categorization from imbalanced MRI dataset using weighted loss and deep feature fusion. Neurocomputing 2023, Volume 520, pp. 94–102.
[11] Muksimova, S.; Umirzakova, S.; Mardieva, S.; Iskhakova, N.; Sultanov, M.; Cho, Y. I. A lightweight attention-driven YOLOv5m model for improved brain tumor detection. Computers in Biology and Medicine 2025, Volume 188.
[12] Passa, R. S.; Nurmaini, S.; Rini, D. P. YOLOv8 based on data augmentation for MRI brain tumor detection. Scientific Journal of Informatics 2023. Volume 10, Issue 3.
[13] Noreen, N.; Palaniappan, S.; Qayyum, A.; Ahmad, I.; Alassafi, M. O. Brain Tumor Classification Based on Fine-Tuned Models and the Ensemble Method. Computers, Materials & Continua 2021, Volume 67, Issue 3, pp. 3967–3982.
[14] Sowrirajan, S. R.; Balasubramanian, S.; Raj, R. S. P. MRI brain tumor classification using a hybrid VGG16-NADE model. Brazilian Archives of Biology and Technology 2023, Volume 66.
[15] Khan, S. U. R.; Zhao, M.; Asif, S.; Chen, X. Hybrid-NET: A fusion of DenseNet169 and advanced machine learning classifiers for enhanced brain tumor diagnosis. International Journal of Imaging Systems and Technology 2024, Volume 34, Issue 1.
[16] Figshare brain tumor dataset. Available online: https://figshare.com/articles/dataset/brain_tumor_dataset/1512427/5 (accessed 08.01.2025).
[17] Br35H: brain tumor detection. Available online: https://www.kaggle.com/datasets/ahmedhamada0/brain-tumor-detection (accessed 08.01.2025).
[18] Brahim, S. B.; Dardouri, S.; Bouallegue, R. Brain Tumor Detection Using a Deep CNN Model. Applied Computational Intelligence and Soft Computing 2024, Volume 2024, Issue 1.
[19] Kang, J.; Ullah, Z.; Gwak, J. MRI-Based Brain Tumor Classification Using Ensemble of Deep Features and Machine Learning Classifiers. Sensors 2021, Volume 21, Issue 6.
[20] Nizamli, Y.; Filatov, A. MRI brain tumor classification using HOG features selected via impurity-based importances measure. International Journal of Electrical and Electronics Research 2024, Volume 12, Issue 4, pp. 1251–1257.
[21] He, K.; Zhang, X.; Ren, S.; Sun, J. Deep Residual Learning for Image Recognition, arXiv:1512.03385v1 2015.
[22] Huang, G.; Liu, Z.; van der Maaten, L.; Weinberger, K. Q. Densely Connected Convolutional Networks. arXiv:1608.06993v5 2018.
[23] Agrawal, T.; Choudhary, P.; Shankar, A.; Singh, P.; Diwakar, M. MultiFeNet: Multi-scale feature scaling in deep neural network for the brain tumour classification in MRI images. Int J Imaging Syst Technol 2024. Volume 34, Issue 1.
[24] Gupta, I.; Singh, S.; Gupta, S.; Nayak, S. R. Classification of brain tumours in MRI images using a convolutional neural network. Current Medical Imaging 2024, Volume 20, Issue 1, pp. 1–9.